Biogeosciences Discuss., https://doi.org/10.5194/bg-2017-424
Manuscript under review for journal Biogeosciences
Discussion started: 6 November 2017

Evaluation of a new inference method for estimating ammonia volatilisation from multiple agronomic plots

Benjamin Loubet[1,*], Marco Carozzi[1#], Polina Voylokov[1], Jean-Pierre Cohan[2], Robert Trochard[2], Sophie Génermont[1]

1 INRA, UMR ECOSYS, INRA, AgroParisTech, Université Paris-Saclay, 78850, Thiverval-Grignon, France
2 ARVALIS, Institut du Végétal, 91720, Boigneville, France
now at: Agroscope Research Station, Climate and Air Pollution Group, Zurich, Switzerland

* Corresponding author: Benjamin.Loubet@inra.fr

Abstract. Tropospheric ammonia (NH_3) is a threat to the environment and human health and is mainly emitted by agriculture. Ammonia volatilisation following application of nitrogen in the field accounts for more than 40% of the total ammonia emissions in France. This hence represents a major loss of nitrogen use efficiency which needs to be reduced by appropriate agricultural practices. In this study we evaluate a novel method to infer ammonia volatilisation from small agronomic plots made of multiple treatments with repetition. The method is based on the combination of a set of ammonia diffusion sensors exposed for durations of 3 hours to 1 week, and a short-range atmospheric dispersion model, used to retrieve the emissions from each plot. The method is evaluated by mimicking ammonia emissions from an ensemble of 9 plots with a resistance-analogue-compensation-point surface exchange scheme over a yearly meteorological database separated into 28-days periods. A multi-factorial simulation scheme is used to test the effects of sensor number and heights, plot dimensions, source strengths and background concentrations, on the quality of the inference method. We further demonstrate by theoretical considerations in the case of an isolated plot that inferring emissions with diffusion sensors integrating over daily periods will always lead to underestimations due to correlations between emissions and atmospheric transfer. We evaluated these underestimations as -8% ± 6% of the emissions for a typical western European climate. For multiple plots, we find that this method would lead to median underestimations of -16% with an interquartile [-8% -22%] for two treatments differing by a factor of up to 20 and a control treatment with no emissions. We further evaluate the methodology for varying background concentrations and ammonia emission patterns and demonstrate the low sensitivity of the method to these factors. The method was also tested in a real case and proved to provide sound evaluations of ammonia losses from surface applied and incorporated slurry. We hence showed that this novel method should be robust and suitable for estimating ammonia emissions from agronomic plots. Further work should anyway be produced for validating this method in real conditions.

Keywords: NH_3 emission, multiple sources, dispersion modelling, experimental design, diffusive samplers

Introduction

Tropospheric ammonia (NH_3) is mainly emitted by agriculture and has great environmental impacts (atmospheric pollution, eutrophication, reduction of biodiversity) which are increasingly taken into account in European and international regulations (Council, 1996; Council, 2016; UNECE, 2012). Ammonia losses also have great agronomic and economic impacts for farmers, as it reduces nitrogen use efficiency. The varying

prices of mineral fertilizers and concerns about environmental and health threats demand improvements in the efficiency of nitrogen utilisation, and especially in recycling nitrogen through organic fertilization (Sutton et al., 2011). Indeed, NH_3 volatilization during storage of manure and slurry and following their field application is the main source of NH_3 in Europe (55.3% of the emissions) and France (48-65%) while farm buildings emissions represent 44.7% and 25-50% in Europe and France, respectively (CITEPA, 2017; ECETOC, 1994; EUROSTAT, 2012; Faburé et al., 2011). Reducing NH_3 losses from this agricultural sector is therefore a major objective for applied research.

While NH_3 emissions from farm buildings and storage can be handled by engineering solutions, losses during organic fertilisation are much more dependent on the combination of application methods (splash plate, band spreading, pressurised injection, open and close slot injection, trailing hose and trailing shoe), soil type and occupation, and environmental conditions (soil humidity, air temperature, wind speed, solar radiation) (Sommer et al., 2003). For instance, Sintermann et al. (2012) report NH_3 losses following cattle and pig slurry application in the field ranging from a few percent to 50% over large fields and up to 100% over medium fields. Evaluating ammonia losses from field fertilisation over a range of practices, soil and climatic conditions is therefore key in evaluating the best application methods.

However, characterising these emissions at the field scale requires complex experimental design and most of the time large fields (Ferrara et al., 2016; Ferrara et al., 2012; Flechard and Fowler, 1998; Loubet et al., 2012; Milford et al., 2009; Sintermann et al., 2011b; Spirig et al., 2010; Sun et al., 2015; Whitehead et al., 2008). Especially useful for measuring ammonia losses are methods that can deal with small and medium-scale fields like agronomic trials (squares of 20 to 50 m on the side), which are widespread. Indirect estimation methods (soil nitrogen balance or ^{15}N balance) are not well adapted to evaluate gaseous ammonia losses, mainly because of the soil heterogeneity and also because the method relies on evaluating small variations of large numbers (McGinn and Janzen, 1998). Among existing methods for measuring NH_3 emissions, the integrated horizontal flux method (Wilson and Shum, 1992) is well adapted, but is a subject of debate in its practical application since it seem to be systematically biased towards higher estimates (Häni et al., 2016; Sintermann et al., 2012). Alternatively, enclosure methods proved to be not representative for a sticky compound such as ammonia (Pacholski et al., 2006), but more concerning is the fact that ammonia fluxes result from an air-surface equilibrium which is disturbed by the confined environment offered by the chamber. Inverse dispersion modelling approaches either based on backward Lagrangian Stochastic models (Flesch et al., 1995) or Eulerian models (Kormann and Meixner, 2001; Loubet et al., 2001), based on the Philip equation (Philip (1959) have been demonstrated to be adapted for estimating NH_3 volatilization from intensive sources (Loubet et al., 2010; Sommer et al., 2005).

These approaches are well adapted to small or medium fields ($\leq$ 50×50 m^2) but typically require hourly concentrations. Long term concentration measurements of NH_3 are now well handled by the use of short path passive samplers developed by Sutton, et al. (2001), or active denuders, which have both been used for concentration monitoring for years (Tang et al., 2001; Tang et al., 2009). These active denuders can be adapted for measuring fluxes based on conditional sampling like the conditional time averaged gradient method COTAG (Famulari et al., 2010), which is a useful method but only adapted for large fields ($\geq$ 0.5 ha). The passive samplers have also been shown to be adapted for inverse modelling estimations of NH_3 sources for large fields (Carozzi et al., 2013b; Ferrara et al., 2014).

In another field of research, solutions to the multiple source problem, which consists of inferring multiple sources based on measured concentrations at multiple points in space and time, have been developed especially since 2008 (Crenna et al., 2008; Gao et al., 2008; Gericke et al., 2011; Mukherjee et al., 2015; Vandré and Kaupenjohann, 1998). They have chiefly been used over regional scales (Flesch et al., 2009; Lushi and Stockie, 2010; Yee and Flesch, 2010), and have been shown to be very dependent on the source-sensor geometry (Crenna et al., 2008; Flesch et al., 2009; Wang et al., 2013). Mukherjee et al. (2015) highlighted the dependency of the inferred source to background concentration and plot disposition, by means of an inverse footprint approach. Yee et al. (2008) have shown how to retrieve the number, location and intensity of multiple sources with dispersion models coupled with Bayesian inference methods. Yee and Flesch (2010) have evaluated the inversion and inference methods for determining 4 points sources using several laser transects. Flesch et al. (2009) have shown that source-receptor geometry is critical in determining whether a multiple-source inversion problem can provide realistic solutions or not. Flesch et al. (2009) have moreover shown that if the geometry is well chosen the accuracy of the method for 15 min data can reach 10% to 20%. These studies have also shown that the multiple source inversion problems can be solved if not ill-conditioned (ill-conditioning depends on the location of sources and concentration sensors and is characterised by a conditioning number κ).

In this study, we pose the following research questions: **"Can inverse dispersion modelling approaches be used for inferring NH_3 emissions from multiple small plots (agronomic trials) using passive samplers, and to which degree of accuracy?"** The answer is given through the investigation of the optimal design in terms of field dimensions, plots locations and size, passive sampler locations and their duration of exposure. Throughout this study, agronomic trials are considered as adjacent multiple small fields with repetitions of *treatments*. A typical trial would consist of three repetitions of three treatments. Hence the double challenge that we face in this study is (i) to consider together the multiple source issue (adjacent small fields) and the (ii) time-integration issue (using passive samplers).

To answer these questions, we use a 4 step approach: (1) The ammonia emissions are first modelled on each source using prescribed NH_3 emission potential dynamics coupled with a simple soil-vegetation-atmosphere exchange scheme to mimic realistic seasonal, daily and hourly variations in NH_3 emissions. (2) These prescribed emissions are then used to estimate the concentration at each target location using short-range atmospheric dispersion modelling over half hourly periods. (3) The obtained concentrations are then averaged over several integration periods to simulate the behaviour of passive samplers. Finally, (4) the sources are evaluated by inference with dispersion modelling based on the averaged concentrations.

Two dispersion models and several inference methodologies are evaluated. The effect of the size of the source, the locations of targets, the dynamics and magnitude of each source and the meteorological conditions are evaluated and discussed. The feasibility of the method is finally evaluated over a real case with two repetitions of three treatments (slurry spreading, injection and a reference without fertilisation).

2. Materials and methods

At first we present the theoretical background of source inference by optimisation for single and multiple sources with time averaging concentration sensors. Then the method used to generate a realistic ammonia source is explained and the dispersion models used for generating the concentration fields and inferring back the sources

are presented. The geometry of the sources and sensors and the meteorological data used are then shown, and finally the real test case used for evaluating the method is detailed.

2.1 The theory of the source inference method

At first we will recall some important theoretical features of the "inverse dispersion modelling" approach which is actually an inference method.

2.1.1 Case of a single area source and a single concentration sampler

We first consider the case of a single area source with a single concentration sampler (target). The source is varying with time. The method is based upon the general superimposition principle (Thomson et al., 2007), which relates the concentration at a given location $C(x,t)$ to the source strength $S(t)$ and the background concentration $C_{bgd}(t)$ using a transfer function $D(x,t)$, which has the dimensions of a transfer resistance (s m^{-1}).

$$C(x,t) = D(x,t) \times S(t) + C_{bgd}(t) \quad (1)$$

Here x denotes the location of the sensor and t the time. The superimposition principle implies that the studied tracer must be conservative, which is a reasonable hypothesis for NH_3 whose reaction time with acids in the atmosphere is below the transport time for spatial scales below 1000 m (Nemitz et al., 2009). Moreover, in **Eq. (1)**, we assume a spatially homogeneous area source with strength $S(t)$. The spatial homogeneity of the source is less trivial for NH_3 as the source itself depends on the concentration at the surface. However (Loubet et al., 2010) have shown that the heterogeneity of the source can be neglected as long as the dimension of the source is larger than 20 m. Hence, this study is limited to source areas with fetch larger than 20 m and a spread of the concentration samplers over a domain smaller than 1000 m. Moreover, it is interesting to note that for infinitely spread fields, the transfer resistance is linearly linked to the transfer matrix (See supplementary material S1)

2.1.2 Effect of time averaging sensors on source inference for a single source

Since we consider time averaging concentration samplers, we develop the time-averaged equation of **Eq. (1)** over a time period τ :

$$\overline{C(x)}^{\tau} = \overline{D(x) \times S}^{\tau} + \overline{C_{bgd}}^{\tau} \quad (2)$$

where the overbars denote a time average over the period τ. Similarly as what is done in turbulent flux calculations, the first part of the right hand side of **Eq. (2)** is decomposed using the Reynolds decomposition of a random variable (Kaimal and Finnigan, 1994), giving:

$$\overline{C(x)}^{\tau} = \overline{D(x)}^{\tau} \times \overline{S}^{\tau} + \overline{C_{bgd}}^{\tau} + \overline{D'(x)S'}^{\tau} \quad (3)$$

Biogeosciences Discuss., https://doi.org/10.5194/bg-2017-424
Manuscript under review for journal Biogeosciences
Discussion started: 6 November 2017

where $\overline{D(x)'S'}^{\tau}$ is the time covariance between $D(x,t)$ and $S(t)$. If the averaged background concentration $\overline{C_{bgd}}^{\tau}$ is a known quantity, **Eq. (3)** can be easily manipulated to give an estimation of the averaged source strength $\bar{S}^{\tau}$, the quantity we want to infer:

$$\bar{S}^{\tau} = \frac{\overline{C(x)}^{\tau} - \overline{C_{bgd}}^{\tau}}{\overline{D(x)}^{\tau}} - \frac{\overline{D'(x)S'}^{\tau}}{\overline{D(x)}^{\tau}} \quad (4)$$

(I) (II)

In the right hand side of **Eq. (4)**, (I) can be calculated from measured $\overline{C_{bgd}}^{\tau}$ and $\overline{C(x)}^{\tau}$ and $\overline{D(x)}^{\tau}$ which is itself calculated with dispersion models. On the contrary (II) is *a priori* unknown and depends on the correlation between the source strength and the transfer function $\overline{D(x)'S'}^{\tau}$. Hence, if (II) is neglected, the inferred source $\bar{S}^{\tau}$ is biased. The relative bias of the method is then:

$$\frac{\delta\bar{S}^{\tau}}{\bar{S}^{\tau}} = \frac{\overline{D'(x)S'}^{\tau}}{\overline{D(x)}^{\tau} \times \bar{S}^{\tau}} \quad (5)$$

Hence we show in **Eq. (5)** that time-averaging leads to a relative bias which can be quantified by the time covariance between the transfer function and the source strength. However this quantity is by nature unknown since the dynamics of $S(t)$ is unknown. Determining $\overline{D(x)'S'}^{\tau}$ requires knowledge of the source dynamics which can be obtained from measurements with a micrometeorological method. It can alternatively be approached by modelling using the state of the art of ammonia exchange processes as we do here.

Additionally to the bias, which is term (II) in **Eq. (4)**, evaluating term (I) is encompassed with errors related to the uncertainties in $\overline{C_{bgd}}^{\tau}$, $\overline{C(x)}^{\tau}$ and $\overline{D(x)}^{\tau}$. In particular, cases when $\overline{D(x)}^{\tau}$ is small may lead to large errors in inferring the source term *S*. This is linked to the conditioning of the inverse problem and is discussed in supplementary material S2.

2.1.3 Case of multiple sources and multiple concentration samplers with time averaging

If we generalise the approach to multiple sources and multiple receptors, then the transfer function becomes a matrix $D(x_i, S_j, t)$, which is the contribution of source S_j to concentration at target located at x_i. For reading purposes we simplify the matrix notation to $D_{i,j}$. **Eq (3)** then becomes:

$$\overline{\begin{bmatrix} C_1 \\ \vdots \\ C_M \end{bmatrix}}^{\tau} = \overline{\begin{bmatrix} D_{1,1} & \cdots & D_{1,M} \\ \vdots & \ddots & \vdots \\ D_{N,1} & \cdots & D_{N,M} \end{bmatrix}}^{\tau} \times \overline{\begin{bmatrix} S_1 \\ \vdots \\ S_M \end{bmatrix}}^{\tau} + \overline{C_{bgd}}^{\tau} + \overline{\begin{bmatrix} D'_{1,1} & \cdots & D'_{1,M} \\ \vdots & \ddots & \vdots \\ D'_{N,1} & \cdots & D'_{N,M} \end{bmatrix}}^{\tau} \times \begin{bmatrix} S'_1 \\ \vdots \\ S'_M \end{bmatrix} \quad (6a)$$

Which in condensed notation gives:

$$\overline{C(x_i)}^{\tau} = \overline{D_{i,J}}^{\tau} \times \bar{S}_J^{\tau} + \overline{C_{bgd}}^{\tau} + \overline{D'_{i,J} \times S'_J}^{\tau} \quad (6b)$$

Biogeosciences Discuss., https://doi.org/10.5194/bg-2017-424
Manuscript under review for journal Biogeosciences
Discussion started: 6 November 2017

If the number of targets is equal to the number of sources, the problem can be solved by inversion of a linear system. If the number of targets is larger than the number of sources, the problem is a multiple linear regression type with unknowns $\overline{S_j}^{\tau}$ and $\overline{C_{bgd}}^{\tau}$. The third term on the right hand side of the **Eq. (6b)** is a bias which is *a priori* unknown and which we will evaluate in this study.

2.1.4 Source inference methods

The inferred sources, $\overline{S_i^{inferred}}^{\tau}$, were derived from **Eqns. (3)** or **(6)** assuming the covariance term (last term on right hand side) was null. The method used to infer the source was either a simple division (**Eq. (3)**) or an optimisation of the linear system using the linear model function *lm* in R (package stats, R version 3.2.3), with either $M = 1$ (single source) or $M = 9$ (multiple sources):

$$\overline{\begin{bmatrix} D_{1,1} & \cdots & D_{1,M} \\ \vdots & \ddots & \vdots \\ D_{N,1} & \cdots & D_{N,M} \end{bmatrix}}^{\tau} \times \overline{\begin{bmatrix} S_1^{inferred} \\ \vdots \\ S_M^{inferred} \end{bmatrix}}^{\tau} = \overline{\begin{bmatrix} C_1 \\ \vdots \\ C_N \end{bmatrix}}^{\tau} - \overline{C_{bgd}}^{\tau} \quad (7)$$

The bias δS_i^{τ} was then evaluated as the difference between the inferred sources $\overline{S_i^{inferred}}^{\tau}$ and the modelled sources $\overline{S_i^{obs}}^{\tau}$ averaged over each period:

$$\delta S_i^{\tau} = \overline{S_i^{inferred}}^{\tau} - \overline{S_i^{obs}}^{\tau} \quad (8)$$

As shown in **Eqns. (3)** and **(6)** the overall mean bias δS_i^{τ} contains (i) a bias term due to the inference method which is dependent mainly on the conditioning of the matrix D_{ij} (see supplementary material S2) and (ii) a bias term which is intrinsically linked to the covariance between D_{ij} and S_j (**Eqns. 3** et **6**). Thus, with **Eq. (8)** we evaluate the sum of the two biases without distinction. In order to infer the sources, the elements of the dispersion matrix D_{ij} need to be determined. The next part details how these were estimated with a dispersion model.

2.2 The dispersion model used for determining the transfer matrix D_{ij}

The elements of the transfer matrix $D_{i,j} = D(x_i, S_j, t)$, were calculated using a dispersion model. Indeed, by definition, $D(x_i, S_j, t)$ is the concentration at location x_i and time t generated by a source S_j of strength $S_j(t) = 1$. The FIDES-3D model ("FIDES",(Loubet et al., 2010), based on the analytical solution of the advection-diffusion equation of Philip (1959) was used for that purpose. This model was first compared and tuned with a backward Lagrangian Stochastic dispersion model (the "WindTrax" software, Thunder Beach Scientific, Nanaimo, Canada, (Flesch et al., 1995). The two models and how the FIDES model was tuned are briefly described hereafter and detailed in the supplementary material sections S3 and S4.

The FIDES model is based on the Philip (1959) solution of the advection-diffusion equation, which assumes power law profiles for the wind speed $U(z)$ and the vertical diffusivity $K_z(z)$. This approach also assumes no chemical reactions in the atmosphere and spatial horizontal homogeneity of roughness length (z_0), wind speed (U), vertical (K_z) and lateral (K_y) diffusivity. The dispersion model is detailed in Huang (1979), and Loubet

(2010). The details of the model and the way the transfer function $D(x_i, S_j, t)$ was estimated is detailed in the supplementary material S2.

The Schmidt number which is the ratio of momentum to scalar vertical diffusivity $Sc = Km_z / K_z$ is key in dispersion modelling, as it determines the vertical diffusion rate of scalars. Wilson (2015) demonstrated that bLS and dispersion models like FIDES give different values of *Sc* by constitution. In order to assure consistency of the Phillip (1959) approach with bLS models, considered as references in dispersion modelling, we chose to tune the Philip (1959) model to get the same *Sc* number as in WindTrax as described by Flesch et al. (1995). The details are given in supplementary material S4. The comparison showed that the tuned FIDES model gives very similar concentrations to WindTrax at measurement heights lower than 2 m above the source, although slightly overestimated under stable and neutral conditions and slightly underestimated under unstable conditions. The correlation between the two models is however very high ($R^2 \geq$ ~0.96) meaning that using the tuned FIDES model to characterise source inference performance, will lead to results very similar to WindTrax. Moreover since in this study the same model is used for predicting and for inferring the fluxes the results are self-consistent.

2.3 Ammonia sources from simple SVAT modelling and prescribed emission potentials

In order to evaluate the bias introduced by time averaging the concentrations when inferring single or multiple sources (third term in **Eqns. 3** and **6**), we generated NH_3 emission patterns mimicking the behaviour of real sources as closely as possible. In that prospect, we used the SurfAtm-NH_3 model developed by Personne et al. (2009), which was used for two purposes: (i) evaluating the turbulence parameters (the friction velocity u_*, and the Monin Obukhov length *L*) from the meteorological datasets to parameterise the dispersion models, and (ii) providing the surface temperature $T(z_0)$ and the surface resistances in order to calculate ammonia emission patterns.

The SurfAtm-NH_3 model is a one-dimensional, bi-directional surface-vegetation-atmosphere-transfer (SVAT) model, which simulates the latent (*LE*) and sensible (*H*) heat fluxes, as well as the NH_3 fluxes between the biogenic surfaces and the atmosphere. It is a resistance analogue model separately treating the vegetation layer and the soil layer, and coupling a slightly modified (Choudhury and Monteith, 1988) model of energy balance and the two-layer bi-directional NH_3 exchange model of (Nemitz et al., 2000) with a water balance model. Unless otherwise stated, the surface was considered a bare soil with z_0 = 5 mm, d = 0 m, and LAI = 0.

The ammonia emission patterns were modelled using the resistance approach and assuming atmospheric concentration was zero, which is a reasonable assumption following nitrogen application and leads to patterns mimicking reality, which is what we are seeking here:

$$F = \frac{C_{\mathrm{pground}}}{R_a(z_{ref}) + R_b\{NH_3\}} \quad (9)$$

Where $R_a(z_{ref})$ is the aerodynamic resistance at the reference height z_{ref} = 3.17 m, and $R_b\{NH_3\}$ is the soil boundary layer resistance for ammonia as described in Personne et al. (2009). The ground surface compensation point concentration (C_{pground}) was expressed as a function of Γ, the ratio of NH_4^+ to H^+ concentration in the soil water at the surface, as in Loubet et al. (2012):

Biogeosciences Discuss., https://doi.org/10.5194/bg-2017-424
Manuscript under review for journal Biogeosciences
Discussion started: 6 November 2017

$$C_{\text{pground}} = K_h\{T(z_0)\} \times K_d\{T(z_0)\} \times \Gamma = \Gamma \times 10^{-3.4362+0.0508\,T(z_0)} \quad (10)$$

where K_h and K_d are the Henry and the dissociation constant for NH_3, and $T(z_0)$ is the soil surface temperature. Since we wanted to evaluate the correlation between the transfer function D_{ij} and the source strength S_j, which is the bias in the inference problem (**Eq. 6**), the NH_3 volatilisation was modelled as to reproduce the variety of existing kinetics of NH_3 emissions from fields. In that prospect, three Γ patterns were simulated:

1. a constant $\Gamma = \Gamma_0$, which would mimic background NH_3 emissions from soils;
2. an exponentially decreasing $\Gamma = \Gamma_0 \exp(-4.6\, t / \tau_0)$, which best represents NH_3 emissions following slurry application;
3. a Gaussian $\Gamma = N(\Gamma_0, \sigma_\Gamma)$, which would represent the typical NH_3 emissions following urea application.

Here Γ_0 is the maximum Γ during the period, t is the time in days, τ_0 is the duration of the emission in days. The factor 4.6 was chosen so that when $t = \tau_0$, Γ goes down to 1% of Γ_0. The duration of the emissions was chosen to be four weeks, $\tau_0 = 28$ days. While these Γ patterns gave the weekly trend of NH_3 emissions, the daily patterns were produced by the thermodynamical and turbulence drivers of NH_3 emissions which were explicitly taken into account through the compensation point (**Eq. 10**). To facilitate understanding, in most of the manuscript only the constant Γ was considered, and the effect of modifying the source strength was evaluated in a sensitivity study.

2.4 Spatial set up of the sources, concentration sensors

The sources (plots) were considered as squares with width x_{plot} and aligned south-north. Two configurations were considered: (1) a single source configuration and (2) a multiple-sources configuration which mimics typical agronomic trials with 9 sources (plots) placed next to each other, with three treatments times three repetitions. Each treatment was assigned a value of Γ_0 different from the others, while the three repetitions of the same treatment were assigned the same value of Γ. The concentration sensors (receptors) locations, x_i, were set in the middle of each plot, at several heights z_i. (**Figure 1**).

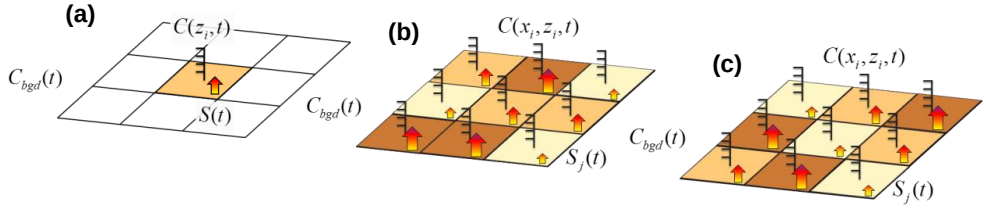

Figure 1. General scheme of the source receptor locations for (a) a single source, and (b) multiple-sources. (c) "optimum" plot layout used for the multiple-source configuration.

A number of plot sizes (x_{plot} = 25, 50, 100 and 200 m on the side), and receptor heights (z_i = 0.25, 0.5, 1 and 2 m), were tested successively. Several source strengths and dynamics were also tested: Γ was first considered constant with time (pattern 1) in all the plots , and the Γ_0 of each of the three treatments were either chosen to be significantly different in strength (10^4, 10^5, 10^6), or of the same order of magnitude (1000, 2000, 4000). Then the three Γ patterns ("constant", "exponential" and "Gaussian") were randomly assigned to the treatments for each

Biogeosciences Discuss., https://doi.org/10.5194/bg-2017-424
Manuscript under review for journal Biogeosciences
Discussion started: 6 November 2017

simulation period. The ammonia background concentration, C_{bgd}, was considered constant and equal to 1 ppb except when studying the sensitivity of the inference method to the background concentration, where it was set as unknown. Throughout this study, an "optimum" block configuration was considered (shown in **Figure. 1c**), which avoided trivial configurations like aligned blocks and maximised the mean distance between blocks.

2.5 Simulation details

2.5.1 Meteorological data and fertiliser application periods

A range of meteorological conditions were simulated based on the half-hourly meteorological data of the FR-Gri ICOS site in 2008. In total 13 periods of 28 days were considered which spanned the whole year except the last two days of the year. Each period consisted of 1344 half-hourly data.

2.5.2 Concentration sensor integration periods

In order to evaluate the influence of the concentration averaging period on the source inference, several integration periods τ were tested: 0.5h (no integration), 3h, 6h, 12h, 24h, 48h, 168h (7 days). In practice the concentrations were computed at each sensor location using **Eq. (6)** over 0.5h: at that frequency, the covariance term is assumed to be negligible. Then the averaged concentrations were computed for all integration periods.

2.5.3 Sensitivity to inferential methods hypotheses

Several hypotheses were considered and summarized in Table 1:

1) the background concentration $\overline{C_{bgd}}^{\tau}$ was either supposed known and fixed to the prescribed values (**C1-C4**) or was inferred (**C5-C7**);
2) the three repetitions of each treatment were either supposed to have the same source strength (**C2**, **C4**, **C5**, **C6**) or they were inferred independently (**C1**, **C3**, **C7**). In **C2**, **C4**, **C5** and **C6**, $S_i = S_m$ for all i and m belonging to the same treatment. In practice a new dispersion matrix was calculated by averaging together all columns belonging to the same treatment (matrix dimension $N \times 3$). Three strength values of S were inferred to be tested;
3) either one concentration sensor at each source location (z_i) was considered (**C1**, **C2**, **C5**) or two sensors positioned at two heights were considered (**C3**, **C4**, **C6**, **C7**). All the measurement heights and their combinations were considered.

Table 1. Hypotheses tested for inferring the sources and background concentration.

Strategy	Number of sensors	Plots[#] have same emissions	Background concentration	Note
C1	1	No	known	Each block is considered independently
C2	1	Yes	known	Each block is considered equal
C3	2	No	known	Identical to C1 except for the number of sensors
C4	2	Yes	known	Identical to C2 except for the number of sensors
C5	1	Yes	unknown	Identical to C2 except for the background concentration estimation
C6	2	Yes	unknown	Identical to C4 except for the background concentration estimation
C7	2	No	unknown	Identical to C3 except for the background concentration estimation

plots are plots having the same treatment (repetitions).

Biogeosciences Discuss., https://doi.org/10.5194/bg-2017-424
Manuscript under review for journal Biogeosciences
Discussion started: 6 November 2017

318 **2.6 Statistical indicators**

319 For each run the mean bias (BIAS), normalised mean bias (NBIAS), were calculated as: $BIAS_i = \frac{1}{N_\tau}\sum_\tau \delta cumS_i^\tau$,
320 $NBIAS_i = BIAS_i / \left(\frac{1}{N_\tau}\sum_\tau cumS_i^{obs}\right)$, where N_τ is the number of the time averaged samples over each 28-day
321 period and $cumS_i$ and $cumS_i^{obs}$ are the cumulated fluxes over the same period. The medians and interquartile of
322 these statistical indicators were then calculated over the 13 periods of 28-days for 2008.

323 **2.7 Real experimental test case**

324 In order to evaluate the feasibility of the method, we applied it to a real test case (**Figure 2**). The trial was
325 located at La Chapelle Saint-Sauveur in France (47°26'44.1"N, 0°58'50.7'W',) and performed from 5th April to
326 26th April 2011 on a bare soil with loamy soil texture. Soil pH in water was 6.2 and the bulk density in the first
327 15 cm was 1.4 t m^{-3}.. The experimental unit consisted of 6 squared sub-plots of 20 m on each side with 2
328 repetitions of 3 treatments: (1) surface application of cattle slurry, (2) surface application and incorporation of
329 the same slurry and (3) no application. The slurry had a pH 7.5, a dry matter (DM) of 6.05%, C:N ratio of 10.4
330 and contained 38.45 g N kg^{-1} (DM) as total nitrogen and 13.25 g N-NH_4 kg^{-1} (DM) as ammoniacal nitrogen.
331 Slurry was applied on 5th April 2011 at a rate of 49 m^3 ha^{-1} which led to 118.7 kg N ha^{-1} and 40.9 kg N-NH_4 ha^{-1}.
332 The application was identical between the repetitions with a small standard deviation (< 0.2 kg N ha^{-1}). The
333 incorporation was performed in two sub-plots one hour after the end of the slurry spreading with a disc harrower
334 at a depth of 0.10 m. The soil humidity between 0 and 5 cm depth was homogeneous over the blocks and
335 decreased from 20±1% to 17±1% w/w between the start and the end of the experiment. The meteorological data
336 were measured nearby (**Figure 2**). Air temperature, relative humidity, global solar radiation, wind velocity and
337 direction were recorded every 30 minutes at 2 m height. The dispersion model input parameters (u_* and L) were
338 evaluated with a simple energy balance model of Holtslag and Van Ulden (1983) assuming a Bowen ratio of 0.5
339 and a deep soil temperature equal the averaged ambient temperature. Ammonia concentration was measured with
340 diffusive samplers (ALPHA samplers), (Sutton et al., 2001; Tang et al., 2001; Tang et al., 2009), which were
341 placed at the centre of each sub-plot at two heights (0.32 and 0.87 m from the ground) as well as next to the
342 assay at three location (5 m away from the plots) at 3 m height. The ALPHA samplers were set in place just after
343 slurry application and incorporation (between 14:20 and 14:50) and left exposed subsequently for 3 h, 22 h, 23 h,
344 23 h, 71 h (3 days) and 359 h (15 days) hence spanning 21 days. The diffusive samplers were prepared prior to
345 the experiment, stored at 4°C in a refrigerator and analysed by colorimetry. Since no background concentrations
346 were measured at a reasonable distance from the field, the background concentration was assumed as the
347 minimum over the whole period of the concentrations measured on the 3 m height masts.

Biogeosciences Discuss., https://doi.org/10.5194/bg-2017-424
Manuscript under review for journal Biogeosciences
Discussion started: 6 November 2017

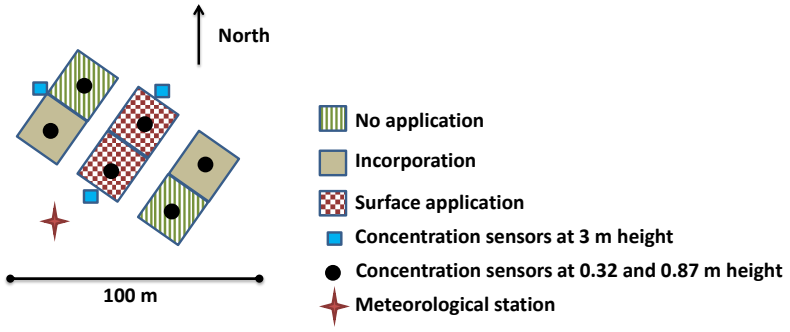

Figure 2. Scheme of the real experimental test case performed on 6 sub-plots with three treatments and two repetitions. Cattle slurry was either applied on the surface or incorporated. The concentration sensor and meteorological station locations are shown on the scheme.

3 Results and discussion

3.1 Meteorological data range and simulated ammonia sources

The meteorological conditions over the 13 periods represented a good sample of temperate climate conditions. In particular u_* and the stability parameter z/L vary over each period and between periods from 0.024 to 1.181 m s^{-1} for u_* and from -49 to 21 m^{-1} for z/L, respectively (**Figure 3**). It is noticeable that u_* showed greater variability during the winter than during the summer, while it was the opposite for z/L. The surface temperature also showed a structure varying between periods, with a larger temperature range during the summer (from 5.7 to 50.4°C) than during the winter (from -5.2 to 22.9°C). This surface temperature variability is an essential feature to representing real case ammonia sources (Sutton et al., 2009), which shows a variability reflecting both the surface temperature and the resistances variations (**Eqns. 9 and 10**).

Biogeosciences Discuss., https://doi.org/10.5194/bg-2017-424
Manuscript under review for journal Biogeosciences
Discussion started: 6 November 2017

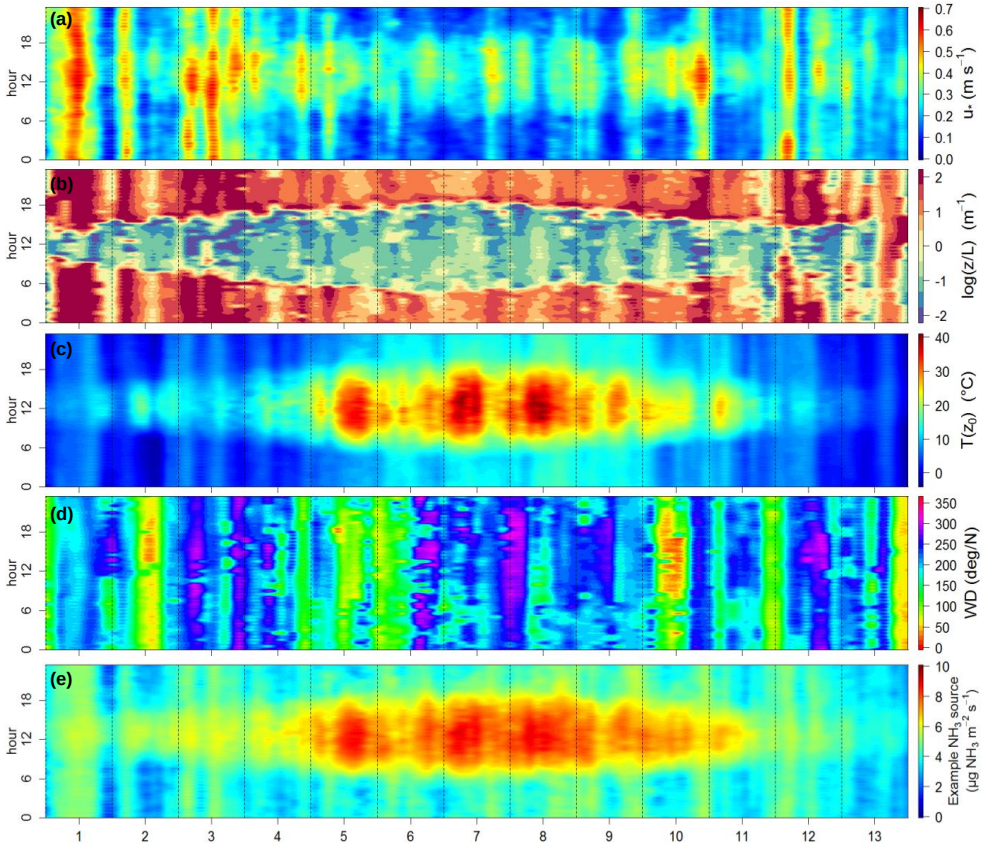

Figure 3. Footprints of measured u_* (a), z/L *at 1 m height* (b), $T(z_0)$ (c), and wind direction (d) for the hour of the day and the 13 considered periods over year 2008 in the FR-GRI ICOS site. The modelled ammonia source is also reported (e) according to Eqns. (9) and (10) over the same period with a Γ = 10000.

3.2 Example ammonia concentration dynamics modelled with the tuned FIDES model

The modelled ammonia concentrations reproduced typical patterns measured above field following nitrogen application well, with maximum concentrations during the day and minimum concentrations at night (**Figure 4**). These patterns are a consequence of daily variations of the sources driven by surface temperature combined with variations in the aerodynamic transfer function D_{ij}, which behaves similarly as a transfer resistance (see supplementary material S1). The integration periods are also shown in **Figure 4,** which illustrates the progressive loss of information of the pattern structure with integration periods. Particularly, it can be seen that the day-to-night variation is captured up to an integration period of 6h. Moreover, it should be noted that averaging also means overestimating lower concentrations and underestimating higher concentrations.

Biogeosciences Discuss., https://doi.org/10.5194/bg-2017-424
Manuscript under review for journal Biogeosciences
Discussion started: 6 November 2017

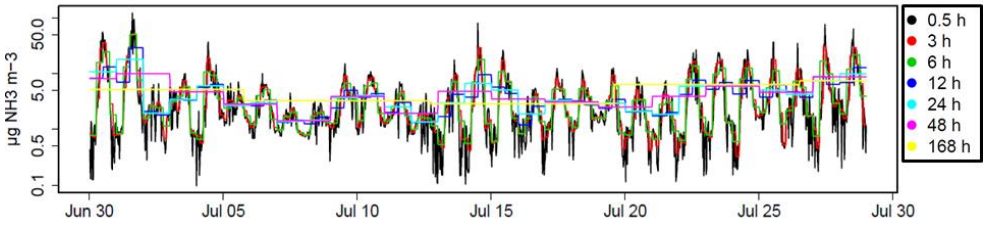

Figure 4. Example modelled concentration pattern at 1 m above a single 50 m width source for several averaging periods (0.5h – 168h) for the month of July 2008. The source Γ was set to 10^5. The y-axis is log scaled.

3.3 Evaluation of the inference method for a single source and a single sensor

At first we evaluate the bias of the inference method for the simpler case of a single source and a single sensor placed in the centre of the source field at several heights, assuming we know the background concentration (strategy **C1**; **Figure 1a.**). This case has the advantage of having a condition number equal to 1 (**Eq. (S1)**) and a bias δS^{τ} which is well defined and equal to $-[\overline{D}^{\tau}]^{-1} \times \left[\overline{D'S'}^{\tau}\right]$ (**Eq. (8)**). This section hence focusses on evaluating the influence of sensor height, time integration, and source dimension on the bias without dealing with the complexity of the interactions between multiple fields.

3.3.1 Example inferred source dynamics

Figure 5 reports an example source inference, which shows the progressive smoothing of the source with integration period. We first see that the source strength corresponding to Γ = 10000 leads to ammonia emissions ranging from 0 to ~1 µg NH_3 m^{-2} s^{-1} in the winter, which corresponds to 0.71 kg N ha^{-1} day^{-1}. Over the entire year, the maximum emission occurs during the hottest days and reaches up to 7.1 kg N ha^{-1} day^{-1}. Regarding the inference method, it can be seen in that example that up to 24 hours the variability in emissions over the period is captured quite well.

Biogeosciences Discuss., https://doi.org/10.5194/bg-2017-424
Manuscript under review for journal Biogeosciences
Discussion started: 6 November 2017

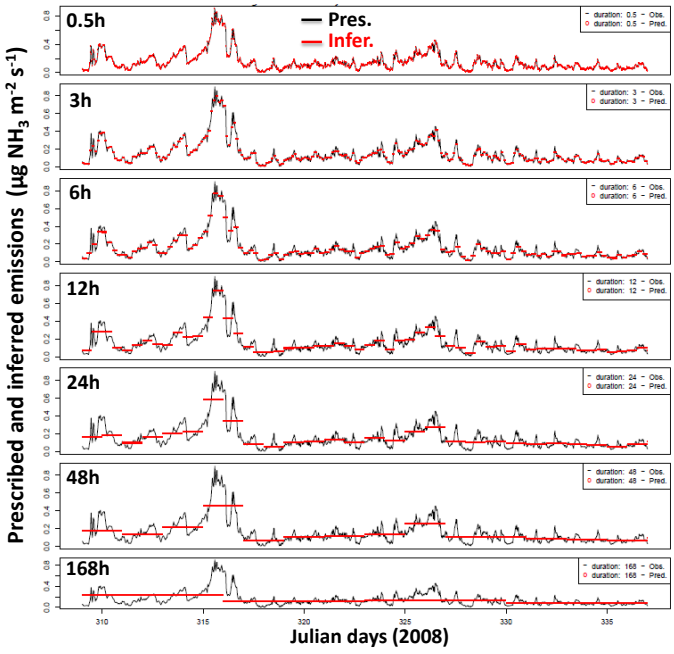

Figure 5. Example source inference for a 25 m width square field and a concentration sensor placed at 0.5 m above ground. Here Γ = 10000 and is set to constant (pattern 1). The 7 integration periods are shown: 0.5h to 168h. The x-axis shows the day of year and corresponds to a span over November. The prescribed source is in black (Obs.) and the inferred one in red (Pred.)

3.3.2 Effect of target height, source dimension and integration period on the bias δS^{τ} for a single source

In this simpler case shown in **Figure 6**, the fractional bias of the inferred emission is mostly negative for the combination where the ratio sensor height / plot dimension is small and integration times are larger than 6h. According to **Eq. (5)**, this means that the covariance term $\overline{D'S'^{\tau}}$ is negative for these conditions, meaning that any increase in source strength S at a time t is correlated with a decrease of the transfer function $D(t)$ and vice versa. This is expected as $S(t)$ increases with the surface temperature (**Eq. (10)**) and is proportional to $\left[R_a\left(z_{ref}\right) + R_b\{NH_3\}\right]^{-1}$ (**Eq. (9)**), while $D(t)$ is proportional to the aerodynamic resistance $R_a(z_{ref})$, as shown in supplementary material S1. Hence, over daily periods, S and D are negatively correlated: S increases during the day and decreases at night (due to temperature and wind speed daily patterns), while D decreases during the day and increases at night (mainly due to wind speed patterns). This is expected to be a general feature for NH_3 surface fluxes as the daily variability reproduced by the model used in this study is representative of most situations from mineral and organic fertilisation, to urine patches or seabird colonies (Ferrara et al., 2014; Flechard et al., 2013; Milford et al., 2001; Moring et al., 2016; Personne et al., 2015; Riddick et al., 2014; Sutton et al., 2013).

The median bias δS_i^{τ} tends to increase in magnitude with the sensor height for large fields (100 and 200 m on side) whilst decreases for smaller fields (25 and 50 m on side) when sensor height gets close to the field boundary layer height. Furthermore, δS_i^{τ} becomes positive and very large when sensors get above the field

Biogeosciences Discuss., https://doi.org/10.5194/bg-2017-424
Manuscript under review for journal Biogeosciences
Discussion started: 6 November 2017

boundary layer height (**Figure 6**). For large fields, the increase of the magnitude of the bias with lower sensor height is expected as *D* decreases with height in absolute value. For small fields, the decrease of the bias corresponds to a loss of information as *D* gets close to zero when the sensor gets closer to the field boundary layer height. For heights above this limit, we observe a change in sign of the bias which can be explained by the fact that the sensor concentration footprint is not in the source during stable conditions (at night) while it is in the source under unstable conditions during the day. The inference method will hence not work if at least one sensor is not below the plot boundary layer height.

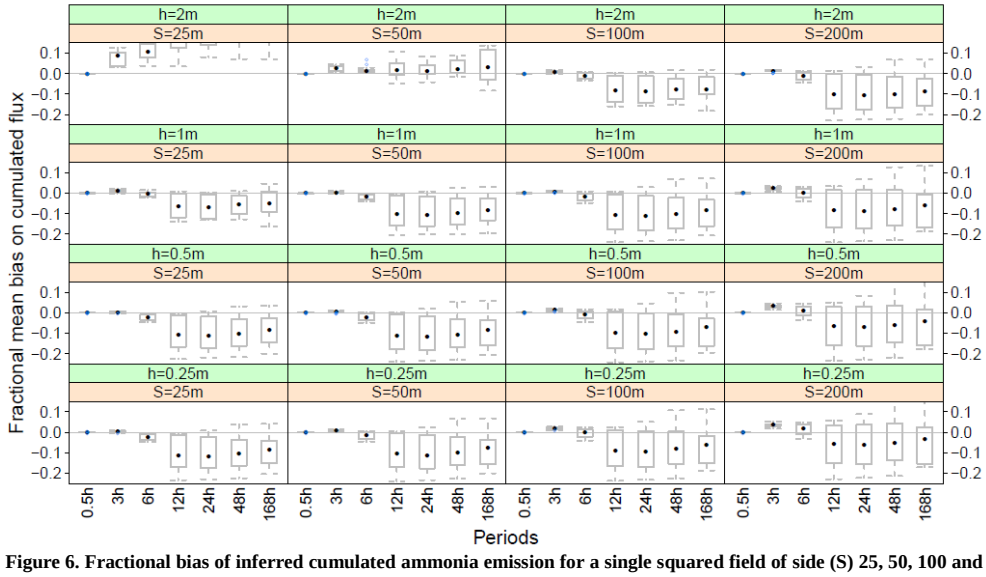

Figure 6. Fractional bias of inferred cumulated ammonia emission for a single squared field of side (S) 25, 50, 100 and 200 m and sensors heights (h) 0.25, 0.5, 1 and 2 m, as a function of the sensors integrating periods from 3 hours to 1 week (168h). The points show the median, the boxes the interquartile and the whiskers the maximum and minimum over the 13 application periods.

We also notice that for integration periods below 3h, the fractional bias is slightly positive, which can be explained by the positive correlation between *S* and *D* at small time scales. This is because of the influence of u_* on $T(z_0)$: for a given solar radiation and air temperature over small time scales (< 3h), an increase in u_* leads to a decrease in $T(z_0)$, which leads to an exponential increase of the surface compensation point according to **Eq. (10)**. However, at the same time, $R_a(z)^{-1}$ decreases, but linearly with u_*. The resulting ammonia emission calculated with **Eq. (9)** nevertheless increases because the exponential effect of temperature overcomes the linear effect of the exchange velocity (data not shown). This effect is more visible for large fields than small fields because over small fields an additional effect is that when u_* decreases, the footprint increases and the source "seen" by the targets hence decreases because it incorporates a fraction of zero emission sources.

Overall, the median fractional bias for weekly integrated emissions over a 25 m field and sensor heights below 0.5 m was overall -8% with an interquartile (-14% to -2%). We can conclude that the bias of the NH_3 emissions is reproducible within ± 6%. We can also conclude that it would be better to place the concentration sensor at a low height to minimise the bias of the method.

443

444 **3.3.3 Effect of surface boundary layer turbulence on the inference method for a single source**

445 The inference method depends on the turbulence at the site and especially on the main drivers of the dispersion
446 which are the friction velocity and the stability regime. Indeed **Figure 7** shows that the relative root mean square
447 residual of the inferred source (RRMSR) decreases with increasing u_* at long integration periods and is larger in
448 slightly stable than near-neutral or slightly unstable conditions. **Figure 7** also shows that the under stable
449 conditions or low u_* the RRMSR increases by more than an order of magnitude (up to 50%) when integration
450 periods increase from 6 to 12 hours, which catches most of the source variance. We also see that under near-
451 neutral or high u_* conditions, the 3rd quartile of the RRMSR remains below 10% for all integration periods.
452 Finally, we also see that the larger 3rd quartiles at short integration periods are obtained with intermediate u_*
453 values or slightly unstable conditions. A similar response of the bias to u_* and $1 / L$ was reported by Figure 6 in
454 (Flesch et al., 2004) and Figure 3 in Gao et al. (2009) in controlled source experiments. While Gao et al. (2009)
455 attributed the bias of the inference method to parameterisation of the stability dependence of the turbulent
456 parameters (z/L), in this study this cannot happen since we use the same parameterisation for prescribing the
457 concentration and inferring it. In our case, the interpretation is to be linked with **Eq. (5)**: the smaller u_* or the
458 most stable conditions also correspond to the larger time-derivatives of source strength (driven by surface
459 temperature and surface exchange resistances) as well as the larger time-derivatives of transfer function D. We
460 hence expect that under such conditions, the covariance between the transfer function and the source strength
461 will be larger than under near-neutral conditions. In a more heuristic view, under low turbulence, large time-
462 derivatives of concentrations are expected above a source due to low mixing (small changes in mixing lead to
463 large variations in concentrations).
464 We conclude that the inference method with a long integration period will lead to very moderate biases for
465 locations with near-neutral conditions and high wind speed, typical of oceanic climates, but may lead to much
466 larger bias under stable conditions and low wind speed typical of continental climates, as soon as the integration
467 period gets up to 12 hours.

Biogeosciences Discuss., https://doi.org/10.5194/bg-2017-424
Manuscript under review for journal Biogeosciences
Discussion started: 6 November 2017

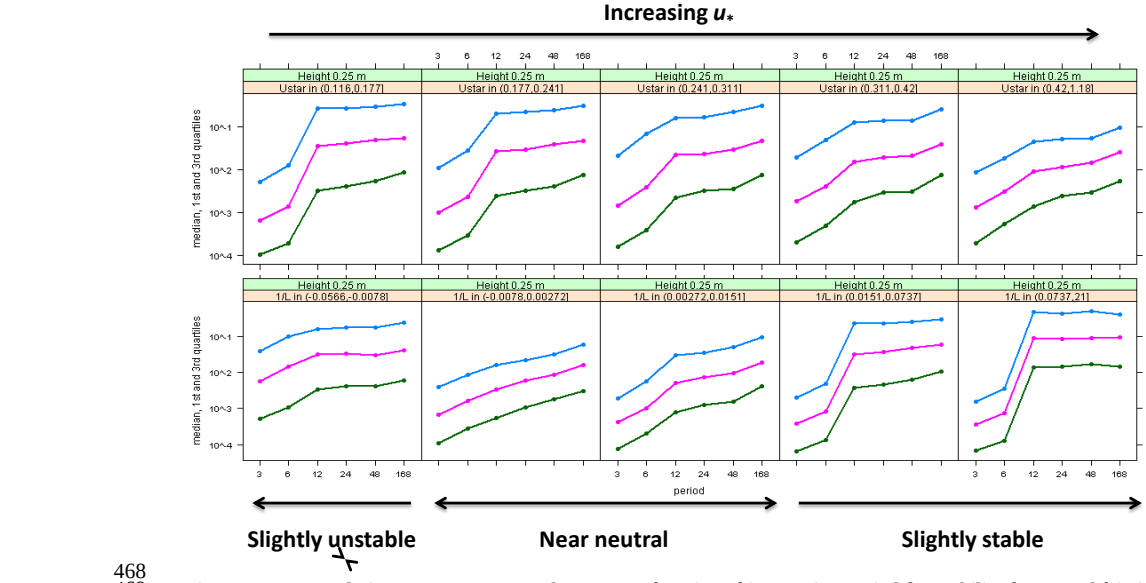

Figure 7. Source relative root mean squared error as a function of integration period for stability factor and friction velocity classes for a single 25 m side field. Medians and quartiles are given for equally sized bins of u_* and $1/L$ and for the lowest sensor height (0.25 m). The blue, pink and green curves are the 3rd, 2nd and 1st quartiles, respectively.

3.4 Multiple source case

In contrast to the single source case, with multiple sources (see **Figure 1b**) the inference method leads to biases at small integration times as can be seen in the example reported in **Figure 8**. In that specific case, the emissions of treatments 2 and 3 are 10 times and 100 times larger than that of treatment 1, respectively. This leads to concentrations over plots of treatment 1 (and to a lesser extent over those of treatment 2) being highly correlated to emissions from plots of treatment 3 (and hence less with sub-plots of treatment 1). As a result, inferring emissions of plots of treatment 1 becomes harder as soon as averaging periods become larger or equal to 3h. This can be viewed as a progressive loss of information of the treatment 1 contribution to concentrations due to the overweighing contribution of treatment 3 plots. However, we also see that treatments 2 and 3 seem quite correctly inferred for integration times smaller than 48h.

Biogeosciences Discuss., https://doi.org/10.5194/bg-2017-424
Manuscript under review for journal Biogeosciences
Discussion started: 6 November 2017

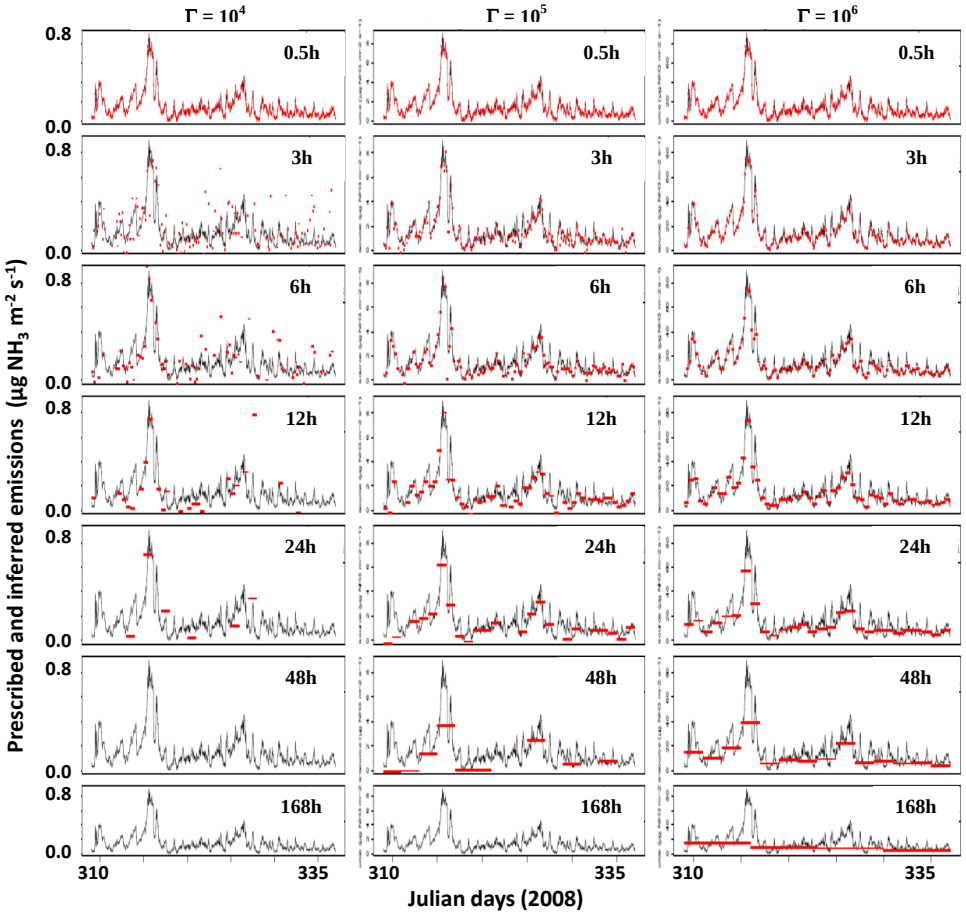

Figure 8. Example result of multiple plot case inference. Black curves: observations; red dots: inferred sources. Left: $\Gamma = 10^4$. Middle: $\Gamma = 10^5$. Right: $\Gamma = 10^6$. Missing red dots are out of the y-scale boundaries. Example plots from treatments 1, 2 and 3 are shown from left to right. The period is the same as in Figure 7 (November 2008 for the FR-Gri ICOS site), and emissions are up to 1, 10 and 100 µg NH_3 m^{-2} s^{-1}, for the three emission potentials. Strategy C7 with target heights 0.25 and 2 m, and source width 25 m on a side.

In the following we will first evaluate the influence of the length of integration periods, sensor heights and plots dimensions on the fractional biases made when inferring the source. Each factor will be evaluated independently of the others in order to understand the processes behind it. For these evaluations background concentration was kept constant at 1 µg NH_3 m^{-3}. Strategy C1 was used except when testing sensor heights for which strategy C3, which uses two targets, was also used. These two strategies assume that the background concentration is known which avoids any compensating effects between source and background concentration inferences. Then the sensitivity of the methodology to the (i) emission ratios between two of the three treatments and (ii) the variability in the background concentration were evaluated. Finally, seven inversion strategies were compared to determine which was the most robust (**Table 1**).

Biogeosciences Discuss., https://doi.org/10.5194/bg-2017-424
Manuscript under review for journal Biogeosciences
Discussion started: 6 November 2017

3.4.1 Effect of integration periods on the bias

We first consider strategy C1, which is the simplest configuration, in which plots are independent, background concentration is known and one target is used above each plot. **Figure 9** shows that for the given treatment range (~1-10-100 µg NH_3 m^{-2} s^{-1}), the fractional mean bias is lower than 0.2 in magnitude for the treatment emitting the most (treatment-3), lower than 0.4 for the intermediate treatment (treatment-2) and up to 8 for the treatment emitting the least (treatment-1); here we considered the 0.25-0.75 quantiles. The bias of the highest treatment (treatment -3) actually behaves similarly to a single source case (**Figure 6**), with a median bias around 10% for 48h integration periods. This is expected because treatment-1 and treatment-2 have much smaller emission strength and hence little influence on the concentration above the treatment-3 plots, which therefore behaves in a similar manner to a single source. As a consequence, this bias in treatment-3 is mainly due to the anti-correlation between *D* and *S* which increases with integration periods. The fractional bias is very large for treatment-1 even for small integration periods. The bias can either be positive or negative showing that this method does not allow for a correct estimation of the smallest sources.

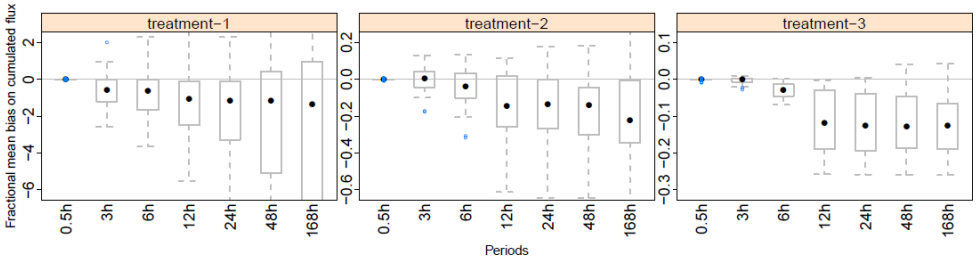

Figure 9. Effect of integration period on source inference in a multiple-plot setup. The fractional mean bias of the source is shown for each treatment (1 to3) corresponding to Γ = 10^4, 10^5, 10^6. Inference strategy C1 was used (single sensor, independent blocks, background concentration known). Statistics for runs with target heights 0.25 and 0.5 m and source side = 25 m are calculated. All application periods are considered. Filled points show medians, boxes show interquartiles and bars show minimums and maximums. Outliers are points to 1.5 times away from boxes limits.

3.4.2 Effect of target heights on the bias

Figure 10 shows that the bias remains quite stable as long as sensor heights are low enough to catch a sufficient part of the field footprint. When only a single height is used (strategy C1) this means that the sensor should be placed at 0.5 m or below for the field size we have tested here (25 m), while for a pair of sensors (strategy C3) the bias remains stable even for sensors places above 0.5 m.

Biogeosciences Discuss., https://doi.org/10.5194/bg-2017-424
Manuscript under review for journal Biogeosciences
Discussion started: 6 November 2017

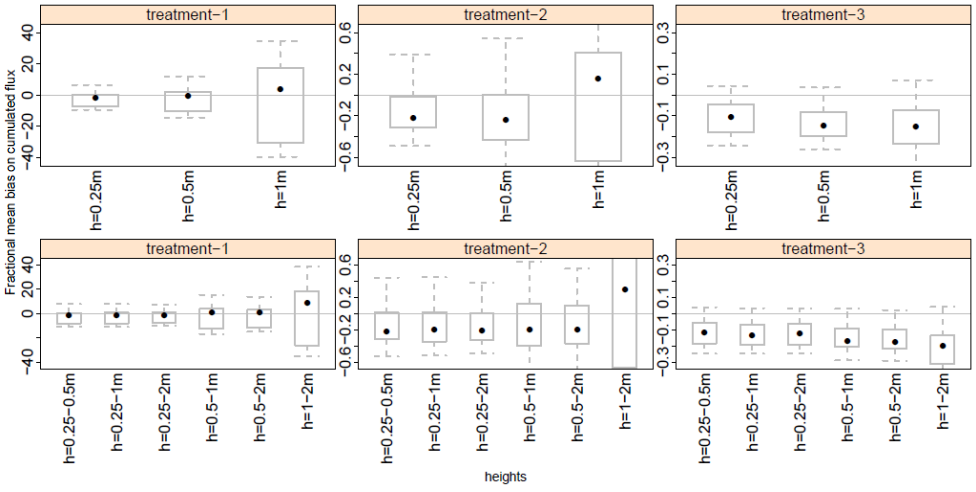

Figure 10. Effect of target heights on source inference in a multiple-plot setup for integration periods of one week (168h). Same as the case reported for Figure 8 except that strategies C1 (with a single sensor) and C3 (with two heights) are compared here (the background is assumed known in both strategies).

3.4.3. Effect of plot size on the bias

Increasing the plot size from 25 to 200 m width reduces the bias of the two largest source treatments for which the median bias reaches values around 10%, while the interquartiles remain stable (**Figure 11**). On the contrary, in treatment-1 (the lowest source), the bias increases. It is expected that the bias in a multiple-source configuration never becomes smaller than the bias in a single source problem which is a limit linked to the time-integration (covariance between the source and the concentration, see **Eqns. (3) and (6)**. It is also expected that the biases remain higher than the single source case until the source size increases sufficiently so that the concentration generated by a block on the neighbour fields become negligible compared to the concentration generated by the source below. This is what we observe in treatment-2 and treatment-3, withtreatment-2 showing a median bias of -13% (larger than in the single source case) for the 200 m large field, while the bias of the highest source tends to be -10% [-17%, -1%], which is the range observed for a single source.

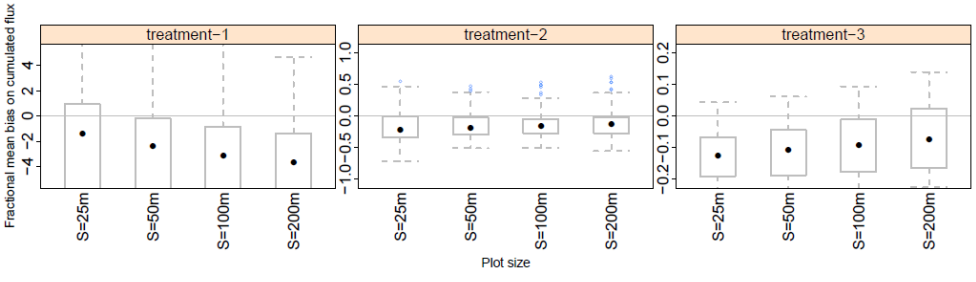

Figure 11. Effect of plots size on source inference in a multiple-plot setup for integration periods of 168h and target heights 0.25 and 0.5 m. Same as in Figure 8.

Biogeosciences Discuss., https://doi.org/10.5194/bg-2017-424
Manuscript under review for journal Biogeosciences
Discussion started: 6 November 2017

544

545 **3.4.4 Sensitivity of the method to ratios of emission potentials between treatments**

546 A central question is the capability of the inference method to resolve small or large differences in emissions
547 from the nearby blocks. Indeed, we can speculate that small differences will be hard to resolve while large
548 differences will lead to large bias. In order to determine the resolution power of the method, we compared the
549 performance of the inference method with a set of three treatments: the first treatment had $\Gamma = 0$ to mimic a
550 reference field receiving no nitrogen. The second treatment had a constant $\Gamma = 1000$ corresponding to a small
551 emission (0.7 kg N ha^{-1} day^{-1}), while in the third treatment Γ was successively set to increasing values from 1500
552 to 10^5 (70 kg N ha^{-1} day^{-1}). In this section we consider that the background is known (sensitivity to the
553 background concentration will be evaluated in the next section).
554 **Figure 12** shows the median and interquartile biases of the cumulated emissions for the longest integration
555 period 168h over the ratio of the high-to-low source treatments. The bias of the highest source always remained
556 around 14%, which is larger than the single source case. The bias of the lowest source increased with increasing
557 inter-treatments source ratio from 13% to 40%. In fact we find that the fractional bias increased approximately as
558 a power function of the ratio of the two predicted sources (dotted lines, $0.11\ x^{0.256}$).
559

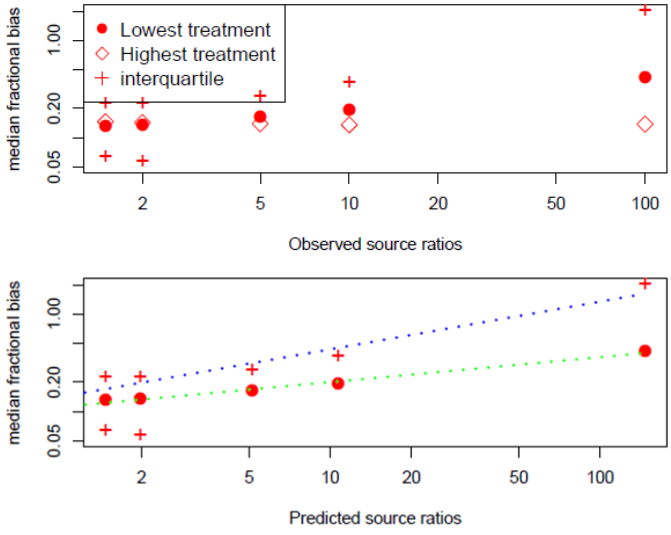

560

561 **Figure 12. Right: Median fractional bias of cumulated emissions as a function of the ratio of the high-to-low source**
562 **treatments for a 7 days integration period. Top: bias as a function of the theoretical source ratios. Bottom: bias as a**
563 **function of the predicted source ratios. Dotted lines show power functions regressions on medians (green) and**
564 **interquartile (blue). Strategies C1 and C3 are pooled together with all runs including sensor heights 0.25 and 0.5 m**

565

566 **3.4.5 Quality of background concentration estimations**

567 As pointed out by Flesch et al. (2004), the knowledge of the background concentration is essential in a source
568 inference problem. Retrieving the background necessitates having at least $N_{sources}+1$ sensors. Hence only
569 strategies with two heights per plot or which assume identical emissions in treatment repetitions can be evaluated

Biogeosciences Discuss., https://doi.org/10.5194/bg-2017-424
Manuscript under review for journal Biogeosciences
Discussion started: 6 November 2017

in their capacity of retrieving the background (strategy C2 to C7). In order to evaluate the sensitivity of the method when the background concentration varies with time, we set a realistic background concentration as a linear combination of u_* and air temperature (T_a) with a mean of 6 µg NH_3 m^{-3}, and a standard deviation of 0.1 µg NH_3 m^{-3}. This test was performed with a range of treatments in order to elucidate the correlations between varying background and varying treatments. We see in **Figure 13** that the concentration, which follows a realistic pattern, is well retrieved, even over the longest period. However, we see that for the treatments with the largest source contrast (Γ = 1000 and 10^5), the background concentration can be overestimated even for small integration periods (6h). The median residual of the background concentration was smaller in magnitude than 0.05 µg m^{-3}, except for the case with very large differences between treatments (0, 1000, 10000), for which the residual reached 0.1 and 0.5 for the 6h and 24h/168h integration periods. Furthermore, the background concentrations were overestimated for the largest source ratios and underestimated for the lowest source ratios and longer integration periods (24h and 168h).

Figure 13. Background concentrations prescribed (Observation) and inferred using strategy C7 and height combination (0.25 m, 2 m): (a) effect of the treatment contrasts for a short integration period of 6h (treatments 1, 2 and 3 are given; (b) effect of integration period for contrasted treatments (Γ = 0, 1000, 10000); (c) effect of integration period for similar treatments (Γ = 0, 1500, 2000).

3.4.6 Identifying the most robust strategy

Finally to identify which strategy is the most suitable for retrieving the emissions, we compare all strategies on a simulation with a variable background (set as in the previous section) and two sources ratios of 2 and 20 between treatments 2 and 3 (treatment 1 being a zero source reference). We found, as expected, that strategies with known backgrounds have low biases compared to strategies that calculate the background except for the strategy C7 which provided biases similar to strategy C3 which is the strategy equivalent to C7 but with known background (**Figure 14**). We also see that incorporating some knowledge of the sources by assuming plots from the same treatment have the same emissions, gave slightly better estimates when the background is known (strategies C2 and C4 compared to C3). This is however not true when the background is unknown, in which case the magnitude of the bias increases up to a median of 0.7 (strategies C5 and C6 compared to C7). It is due to compensation between background concentration and source strength as we have seen in **Figure 14,** that the

Biogeosciences Discuss., https://doi.org/10.5194/bg-2017-424
Manuscript under review for journal Biogeosciences
Discussion started: 6 November 2017

600 background concentration was overestimated in such cases. We also see, as expected, that the strategies with two
601 sensors placed at different heights above each plot lead to better evaluations of the emissions. Overall, the
602 strategy based on two sensors above each plot, which also assumes that sources are independent, seems to be the
603 most robust (strategy C7). This strategy does not assume the background is known, nor does it assume the plots
604 have similar emissions, which is more adapted to reality. Indeed, even though the same amount of nitrogen is
605 applied in each repetition plot, the emission may vary due to soil heterogeneity and advection. We finally get a
606 median bias for strategy C7 which is -16% with an interquartile [-8% -22%]. It is important to stress though that
607 the minimums and maximums are further away, which indicates that under some rarer circumstances, the method
608 may overestimate the sources by 12% or underestimate them by 40%. These cases correspond to integration
609 periods with very low wind speeds and stable conditions.
610

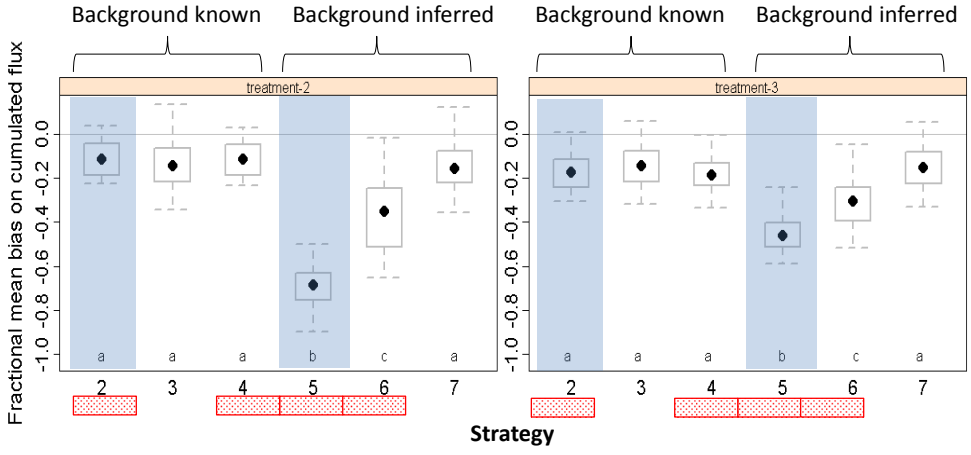

611

612 **Figure 14. Comparison of biases for all source inference strategies. In strategies C2, C3 andC4 we hypothesize that we**
613 **have perfect knowledge of the background concentrations, while in strategies C5, C6 and C7 background**
614 **concentrations are inferred together with the sources. In strategies C2, C4, C5 and C6 (red rectangles) we suppose**
615 **that plots from the same treatment have the same emissions, while in strategy C3 and C7 we infer each plot**
616 **separately. In strategy C2 and C5 we assume single sensors are placed above each plot (blue shades), while in**
617 **strategies C3, C4, C6, C7 we assume two sensors are placed above each plot.**

618

619 **3.5 Application of the methodology to a real test case with multiple treatments**

620 The evaluation of the methodology on a real test case is shown in **Figures 15-17**. The concentration measured
621 above the different treatments shows a much higher concentration above the surface applied slurry (up to
622 200 µg N-NH_3 m^{-3}) than above the two other treatments (below 50 µg N-NH_3 m^{-3}), (**Figure 15**).

Biogeosciences Discuss., https://doi.org/10.5194/bg-2017-424
Manuscript under review for journal Biogeosciences
Discussion started: 6 November 2017

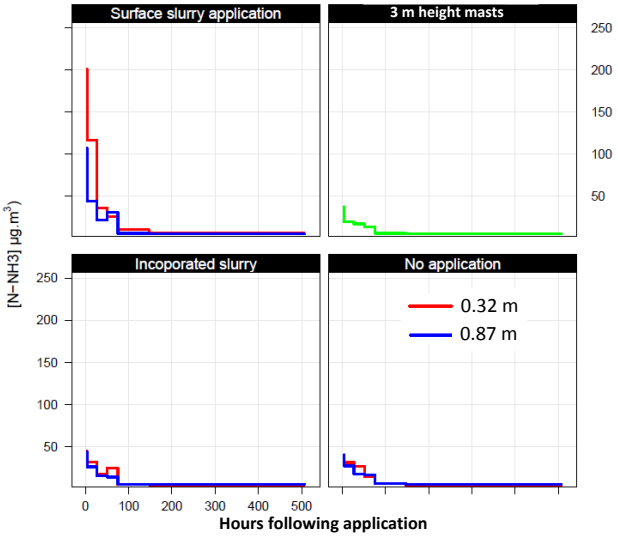

Figure 15. Concentrations measured in a real test case with 6 blocks composed of three treatments and two repetitions. Here the mean concentration for the repetition and the three replicates ALPHA samplers are shown at two heights above ground. The concentration measured at 3 m height at 5 m away from the plots is also shown in green. The background concentration, evaluated as the minimum of the green curve was 5 µg N-NH_3 m^{-3}.

The inference method gives very consistent results both in terms of comparison between repetitions of a given treatment and in terms of comparison between treatments (Strategy C7 shown in **Figure 16**). Emissions above 3 kg N ha^{-1} (3.2 kg N ha^{-1} on average) were found for the surface slurry application with a very good reproducibility between repetitions. This corresponds to an emission factor around 8.2% of the N-NH_4 applied and 2.8% of the total N applied, which is in-line with agronomic references (Sintermann et al., 2011a; Sommer et al., 2006). In contrast, the incorporated slurry showed much smaller and more variable fluxes between -0.2 and 0.25 kg N ha^{-1}. Furthermore, no significant differences were found between the no-application and the slurry incorporation treatments (Student t-Test with p-values larger than 0.03).

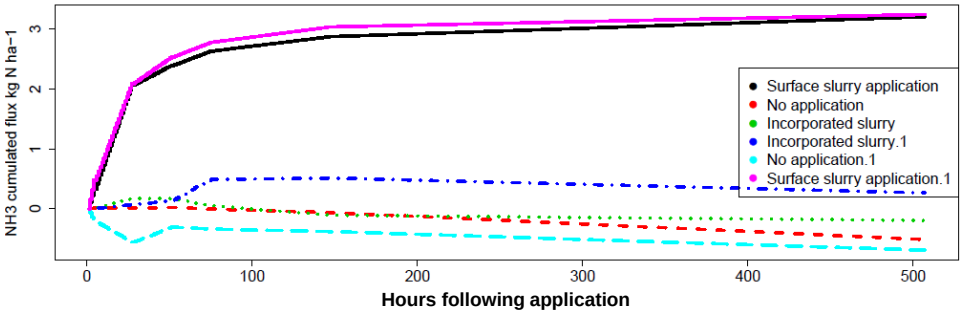

Figure 16. Cumulated fluxes estimated with the inverse method on the real test case with strategy C7. Three treatments with two repetitions are compared.

Biogeosciences Discuss., https://doi.org/10.5194/bg-2017-424
Manuscript under review for journal Biogeosciences
Discussion started: 6 November 2017

Comparing the inference strategies is instructive (**Figure 17**). We see that in methods which assume a known background (strategies C3 and C4), the inferred emissions are higher than when background is assumed unknown. We should remind that we set the background concentration to the minimum concentration measured on the 3 m height masts because these were located too close to the plots to be considered as real background masts. This explains why strategies C3 and C4 lead to higher estimates compared to strategies C6 and C7, as the background may have been underestimated. We also find that all methods consistently infer a deposition flux to the blocks with no application, which is consistent with our knowledge of ammonia exchange between the atmosphere and the ground (Flechard et al., 2013). Indeed, the concentration in the atmosphere, which is enriched by the nearby sources is expected to be higher than near the ground, due to a low soil pH (6.1), a low nitrogen content in the soil surface (6-9.5 g N kg^{-1} DM), and a 20% humid soil surface, hence leading to a flux from the air to the ground.

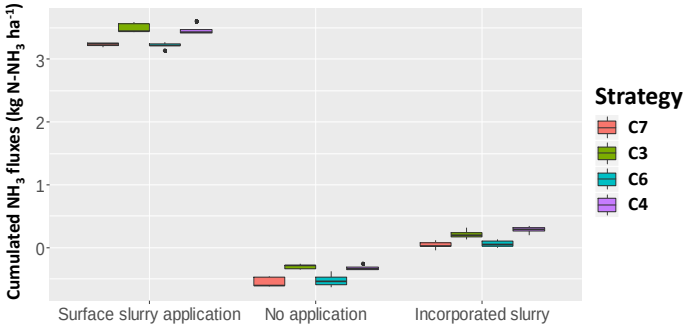

Figure 17. Same as Figure 14 but grouped by treatments and with additional strategies C4 and C6 which consider that replicates have the same surface flux. The variability in the boxplot aggregates the uncertainty on the inference method (the standard deviation on the flux estimate in the least-square model, which accounts for the variability in the replicated concentration measurements), and the variability between the repetitions in each treatment.

From our theoretical study we know that strategy C7 should give a bias around -15 ± 8%. Therefore, we could expect that the real flux is the one measured with C7 times (1.15 ±0.08), hence 3.7 ± 0.25 kg N ha^{-1}. This corresponds to 10.1 ± 0.7 % of the N-NH_4 applied and 3.4 ± 0.2% of the total N applied. For the incorporated slurry, the uncertainty would be much larger and is not evaluated here. We should bear in mind that the theoretical study is based on the median of the simulations done with the 2008 dataset in Grignon which had similar meteorological conditions to this trial. It would be much more relevant in future developments to evaluate the bias based on the same method as developed here but based on the emissions and meteorological conditions of the real case.

3.6 Comparison with previous work

Several studies have reported methodologies for evaluating multiple sources using dispersion models. These were mostly based on Backward Lagrangian modelling (Crenna et al., 2008; Flesch et al., 2009; Gao et al., 2008). There were several inference methods reported: the methods based on the inversion of the dispersion matrix D_{ij} or singular value decomposition of least-square optimisation (Flesch et al., 2009), which optimise the conditioning of the dispersion matrix and one based on Bayesian inference (Yee and Flesch, 2010). Yee et al. (2010) showed that the Bayesian approach would avoid unrealistic source estimates which could appear when

the matrix conditioning was poor. Unrealistic source estimates were for instance reported by Flesch et al. (2009), with negative emission sources.

In Ro et al. (2011), they evaluated the bLS technique to infer two controlled methane surface sources with laser measurements. They found 0.6 recovery ratios (ratio of inferred to known source) if the fields were not in the footprint of the sensor but with adapted filters, they found a high degree of recovery with of 1.1 ± 0.2 and 0.8 ± 0.1 for the two sources respectively. They found that in contradiction to Crenna et al. (2008) and Flesch et al. (2009), even with large conditioning numbers they had high recovery rates.

3.6.1 Sensor positioning and conditioning number

Crenna et al. (2008) have clearly shown that the optimal sensor positioning should be so that each sensor sees preferentially a single source, and reversely, each source should preferentially influence a single sensor. In this study the sources-sensors geometry was especially designed in a way that minimises the condition number *CN*, by placing the sensors in the middle of each plot. For the smallest source (25 m width), the conditioning number ranged from 1.97 to 3.01 (median 2.42) for sensors located at 0.25 m, and increased to 2.6-6.9 (median 3.2) for sensors at 0.5 m, 4.7-150 (median 21) for sensors at 1.0 m, and 40-165000 (median 640) for sensors at 2 m. This shows that including at least one sensor per block at heights lower than the field width divided by 20 would ensure that the conditioning number remains lower than in most trials of Crenna et al. (2008).

By comparing different strategies we have found that the strategies using two sensors over each source systematically led to improved performances (C3 versus C1 and C6 versus C5, **Figure 14**). This is also in line with the results of Crenna et al. (2008), who showed that using more sensors separated spatially improves the performance of the inference method. Hence we can conclude that the inference method we used is based on a well-conditioned system which leads to robust results of the least-square optimisation. This is further illustrated by the real case example (**Figures 15-17**) which shows a good reproducibility between block repetitions. Indeed, good reproducibility between repetitions is a check for evaluating the quality of the inference method in real test cases. The use of Bayesian inference method would however also be valuable in the setup we propose here.

3.6.2 Effect of time integrating sensors on the source inference quality

The use of time averaging sensors for estimating ammonia sources was already reported by Sanz et al. (2010), Theobald et al. (2013), Carozzi et al. (2013a; 2013b), Ferrara et al. (2014) and Riddick et al. (2016a; 2014). All these studies have shown the feasibility of these measurements, however only a few of them allow estimating the impact of averaging: Riddick et al. (2014) measured emissions from a bird colony in the Ascension island with WindTrax using both several alpha samplers in a transect across the colony and a continuous analyser for ammonia (AiRRmonia, Mechatronics, NL) downwind. They also averaged the continuous sampler concentrations to evaluate the effect of averaging on the emissions estimates. They found as we do here that averaging over monthly periods would lead to systematic underestimations from -9% to -66%. They also found that estimations from badges would lead to average underestimations of -12%. This is very close to what we find here for a single source over one week (**Figure 6**). In a similar comparison Riddick et al. (2016b) found that time-integration led to slight overestimations with integration approach, which is within the range of statistics of the bias we have found for the larger area sources (3rd Quartile in **Figure 6**).

3.6.3 Dependency to meteorological conditions

We should bear in mind that the use of time averaging sensors in the inference method is also highly dependent on the surface layer turbulent structure as shown by **Figure 7**. We find, as expected, that stable conditions or low wind speed conditions are those that lead to the highest potential bias (as shown by the 3rd quartile under stable conditions in **Figure 7** bottom). This is a well-known limitation of inverse dispersion modelling which was reported by Flesch et al. (2009; 2004) and which suggested that inverse dispersion would be inaccurate for $u_* < 0.15$ m s^{-1} and $|z/L| < 1$. However, both our study and the studies of Riddick et al. (2014; 2016b) show that this is not as much of an issue for ammonia emissions. Indeed, this is due to the fact that ammonia emissions follow a daily cycle with low emissions at night and high emissions during the day. This is firstly because (1) the ground surface compensation point concentration (C_{pground}) has an exponential dependency on surface temperature as assumed in **Eq. (10)** based on known thermodynamical equilibrium constants (Flechard et al., 2013). This is secondly due to the fact that ammonia emission is a diffusion-based process which is limited by the surface resistances, as modelled in **Eq. (9)**, which leads to small fluxes when $R_a(z_{ref})$ and $R_b\{NH_3\}$ get large, which happens during low wind speeds (they are both roughly inversely proportional to wind speed) and stable conditions, which also happens at night (Flechard et al., 2013). In real situations, the combination of small turbulence and high surface concentration leads to a further decrease of the flux which is dependent on the difference between C_{pground} and the concentration in the atmosphere above (a feature which was not accounted for in this study as this would imply a higher degree of complexity in the modelling approach). This means that the results we found in this study would not apply for species having an emission pattern with a different temporal dynamics (either constant or anti-correlated with surface temperature or wind speed).

4. Conclusions

In this study we have demonstrated that it is possible to infer with reasonable biases ammonia emissions from multiple small fields located near each other using a combination of a dispersion model and a set of passive diffusion sensors which integrate over a few hours to weekly periods. We found that the Philip (1959) analytical model gave similar concentrations as the backward Lagrangian Stochastic model WindTrax (using the Monin and Obukhov parameterisation) above a small source, as long as the stability correction functions used in both models are similar.

We demonstrated by theoretical considerations that passive sensors always lead to the underestimation of ammonia emissions for an isolated source because of the negative time correlation between the ammonia emissions and the transfer function. Using a yearly meteorological dataset typical of the oceanic climate of western Europe we found that the bias over weekly integration times is typically -8±6%, which is in line with previous reports for bird colonies. Larger biases are expected for meteorological conditions with stable conditions and low wind speeds typical of continental climates, as soon as the integration period is larger than 12 hours.

We showed that the quality of the inference method for multiple sources was dependent on the number of sensors considered above each plot. The most essential technique to minimise the bias of the method was to place a sensor in the middle of each source within the boundary layer. The quality of the sensor positioning was evaluated using “condition numbers” which ranged from 2 to 3 for a sensor placed at 25 cm above the ground to

much higher values (40-1.6×10^5) for a sensor at 2 m height above 25 m width sources. Although the highest sensors had low condition numbers, they were shown to improve the robustness of the sources inference especially for evaluating the background concentrations. Using replicates of each treatment was found to be essential for evaluating the quality of the inference and derive robust statistical indicators for each treatment.

When considering a system, characteristic of agronomic trials, composed of a low and a high potential source and a reference with no nitrogen application, we found that the fractional bias remained smaller than around 25% for ratios between the largest to the smallest sources lower than factor 5 and increased as a power function of the ratio. Furthermore, the dynamics of the emissions were found not to strongly affect the fractional bias. As expected, we also found that the fractional bias decreased with increasing source dimensions, especially for the lowest source strength in a multiple source trial.

Finally, a test on a practical trial proved the applicability of the method in real situations with contrasted emissions. We indeed calculated ammonia emissions of around 10.1 ± 0.7% of the total ammoniacal nitrogen applied for surface applied slurry while we found less than 1% emissions for the treatments with incorporated slurry.

This method could also be improved by incorporating knowledge of the surface source dynamics into the inference procedure. Further work is required however, for validating the method, for instance using prescribed emissions, and to evaluate it for growing crops using real measurements with diffusion samplers close to the ground.

Acknowledgements

This study was supported by EU FP7 NitroEurope-IP (grant number 017841) and ECLAIRE (grant number 282910), French national projects CASDAR VOLAT'NH3 (grant number 0933), ADEME EVAPRO (grant number 1560C0036), ADEME EVAMIN (grant number 1660C0012). The data sets used in this paper can be obtained from the authors upon request. The meteorological dataset used in this study are from the ICOS site FR-GRI which can be obtained from http://fluxnet.fluxdata.org/. We thank Erwan Personne for the use of the Surfatm model.

Supplementary material

(see supplementary material manuscript)

References

Carozzi, M., Ferrara, R.M., Rana, G. and Acutis, M., 2013a. Evaluation of mitigation strategies to reduce ammonia losses from slurry fertilisation on arable lands. Sci Total Environ, 449: 126-33.

Carozzi, M., Loubet, B., Acutis, M., Rana, G. and Ferrara, R.M., 2013b. Inverse dispersion modelling highlights the efficiency of slurry injection to reduce ammonia losses by agriculture in the Po Valley (Italy). Agricultural and Forest Meteorology, 171: 306-318.

Choudhury, B.J. and Monteith, J.L., 1988. A four-layer model for the heat budget of homogeneous land surfaces. Q J Roy Meteor Soc, 114: 373-398.

783 CITEPA, 2017. Inventaire des émissions de polluants atmosphériques en France métropolitaine, format CEE-
784 NU. CITEPA 494 / Convention MATE 26 / 2001, Centre Interprofessionnel Technique d'Etudes de la
785 Pollution Atmosphérique.
786 Council, E., 1996. Directive 96/61/EC of 24th September 1996 concerning integrated pollution prevention and
787 control. , European Council, Brussels, Belgium.
788 Council, E., 2016. Directive (EU) 2016/2284 of the European parliament and of the council of 14 December
789 2016 on the reduction of national emissions of certain atmospheric pollutants, amending Directive
790 2003/35/EC and repealing Directive 2001/81/EC, European Council, Brussels, Belgium.
791 Crenna, B.R., Flesch, T.K. and Wilson, J.D., 2008. Influence of source-sensor geometry on multi-source
792 emission rate estimates. Atmospheric Environment, 42(32): 7373-7383.
793 ECETOC, 1994. Ammonia emissions to air in Western Europe, European Centre for Ecotoxicology and
794 Toxicology of Chemicals, Avenue E Van Nieuwenhuyse 4, Brussels.
795 EUROSTAT, 2012. Agroenvironmental indicator - ammonia emission, Eurostat, Luxemburg.
796 Faburé, J. et al., 2011. Synthèse bibliographique sur la contribution de l'agriculture à l'émission de particules
797 vers l'atmosphère : identification de facteurs d'émission, ADEME / INRA.
798 Famulari, D. et al., 2010. Development of a low-cost system for measuring conditional time-averaged gradients
799 of SO2 and NH3. Environ Monit Assess, 161(1-4): 11-27.
800 Ferrara, R.M. et al., 2016. Dynamics of ammonia volatilisation measured by eddy covariance during slurry
801 spreading in north Italy. Agriculture, Ecosystems & Environment, 219: 1-13.
802 Ferrara, R.M. et al., 2014. Ammonia volatilisation following urea fertilisation in an sorghum crop in Italy
803 irrigated. Agricultural and Forest Meteorology, 195: 179-191.
804 Ferrara, R.M. et al., 2012. Eddy covariance measurement of ammonia fluxes: Comparison of high frequency
805 correction methodologies. Agricultural and Forest Meteorology, 158(0): 30-42.
806 Flechard, C.R. and Fowler, D., 1998. Atmospheric ammonia at a moorland site. II: Long-term surface-
807 atmosphere micrometeorological flux measurements. Q J Roy Meteor Soc, 124(547): 759-791.
808 Flechard, C.R. et al., 2013. Advances in understanding, models and parameterizations of biosphere-atmosphere
809 ammonia exchange. Biogeosciences, 10(7): 5183-5225.
810 Flesch, T.K., Harper, L.A., Desjardins, R.L., Gao, Z.L. and Crenna, B.P., 2009. Multi-Source Emission
811 Determination Using an Inverse-Dispersion Technique. Boundary-Layer Meteorology, 132(1): 11-30.
812 Flesch, T.K., Wilson, J.D., Harper, L.A., Crenna, B.P. and Sharpe, R.R., 2004. Deducing ground-to-air
813 emissions from observed trace gas concentrations: A field trial. Journal of Applied Meteorology, 43(3):
814 487-502.
815 Flesch, T.K., Wilson, J.D. and Yee, E., 1995. Backward-Time Lagrangian Stochastic Dispersion Models and
816 Their Application to Estimate Gaseous Emissions. Journal of Applied Meteorology, 34(6): 1320-1332.
817 Gao, Z.L., Desjardins, R.L., van Haarlem, R.P. and Flesch, T.K., 2008. Estimating Gas Emissions from Multiple
818 Sources Using a Backward Lagrangian Stochastic Model. J Air Waste Manage, 58(11): 1415-1421.
819 Gao, Z.L., Mauder, M., Desjardins, R.L., Flesch, T.K. and van Haarlem, R.P., 2009. Assessment of the backward
820 Lagrangian Stochastic dispersion technique for continuous measurements of CH4 emissions.
821 Agricultural and Forest Meteorology, 149(9): 1516-1523.

822 Gericke, D., Pacholski, A. and Kage, H., 2011. Measurement of ammonia emissions in multi-plot field
823 experiments. Biosystems Engineering, 108(2): 164-173.
824 Häni, C., Sintermann, J., Kupper, T., Jocher, M. and Neftel, A., 2016. Ammonia emission after slurry application
825 to grassland in Switzerland. Atmospheric Environment, 125(Part A): 92-99.
826 Holtslag, A.A.M. and Vanulden, A.P., 1983. A Simple Scheme for Daytime Estimates of the Surface Fluxes
827 from Routine Weather Data. Journal of Climate and Applied Meteorology, 22(4): 517-529.
828 Huang, C.H., 1979. A theory of dispersion in turbulent shear flow. Atmospheric Environment, 13: 453-463.
829 Kaimal, J.C. and Finnigan, J.J., 1994. Atmospheric Boundary Layer Flows, Their structure and measurement.
830 Oxford University Press., New York, 289 pp.
831 Kormann, R. and Meixner, F.X., 2001. An analytical footprint model for non-neutral stratification. Boundary-
832 Layer Meteorology, 99(2): 207-224.
833 Loubet, B. et al., 2012. Investigating the stomatal, cuticular and soil ammonia fluxes over a growing tritical crop
834 under high acidic loads. Biogeosciences, 9(4): 1537-1552.
835 Loubet, B. et al., 2010. An inverse model to estimate ammonia emissions from fields. European Journal of Soil
836 Science, 61(5): 793-805.
837 Loubet, B., Milford, C., Sutton, M.A. and Cellier, P., 2001. Investigation of the interaction between sources and
838 sinks of atmospheric ammonia in an upland landscape using a simplified dispersion-exchange model.
839 Journal of Geophysical Research-Atmospheres, 106(D20): 24183-24195.
840 Lushi, E. and Stockie, J.M., 2010. An inverse Gaussian plume approach for estimating atmospheric pollutant
841 emissions from multiple point sources. Atmospheric Environment, 44(8): 1097-1107.
842 McGinn, S.M. and Janzen, H.H., 1998. Ammonia sources in agriculture and their measurement. Canadian
843 Journal of Soil Science, 78(1): 139-148.
844 Milford, C., Hargreaves, K.J., Sutton, M.A., Loubet, B. and Cellier, P., 2001. Fluxes of NH3 and CO2 over
845 upland moorland in the vicinity of agricultural land. Journal of Geophysical Research-Atmospheres,
846 106(D20): 24169-24181.
847 Milford, C. et al., 2009. Ammonia fluxes in relation to cutting and fertilization of an intensively managed
848 grassland derived from an inter-comparison of gradient measurements. Biogeosciences, 6(5): 819-834.
849 Moring, A. et al., 2016. A process-based model for ammonia emission from urine patches, GAG (Generation of
850 Ammonia from Grazing): description and sensitivity analysis. Biogeosciences, 13(6): 1837-1861.
851 Mukherjee, S., McMillan, A.M.S., Sturman, A.P., Harvey, M.J. and Laubach, J., 2015. Footprint methods to
852 separate N2O emission rates from adjacent paddock areas. International Journal of Biometeorology,
853 59(3): 325-338.
854 Nemitz, E. et al., 2009. Aerosol fluxes and particle growth above managed grassland. Biogeosciences, 6(8):
855 1627-1645.
856 Nemitz, E., Sutton, M.A., Schjoerring, J.K., Husted, S. and Wyers, G.P., 2000. Resistance modelling of
857 ammonia exchange over oilseed rape. Agricultural and Forest Meteorology, 105(4): 405-425.
858 Pacholski, A. et al., 2006. Calibration of a simple method for determining ammonia volatilization in the field -
859 comparative measurements in Henan Province, China. Nutrient Cycling in Agroecosystems, 74(3): 259-
860 273.

Personne, E. et al., 2009. SURFATM-NH3: a model combining the surface energy balance and bi-directional exchanges of ammonia applied at the field scale. Biogeosciences, 6(8): 1371-1388.

Personne, E. et al., 2015. Investigating sources and sinks for ammonia exchanges between the atmosphere and a wheat canopy following slurry application with trailing hose. Agricultural and Forest Meteorology, 207: 11-23.

Philip, J.R., 1959. The Theory of Local Advection .1. J Meteorol, 16(5): 535-547.

Riddick, S. et al., 2016a. Estimate of changes in agricultural terrestrial nitrogen pathways and ammonia emissions from 1850 to present in the Community Earth System Model. Biogeosciences, 13(11): 3397-3426.

Riddick, S.N. et al., 2014. Measurement of ammonia emissions from tropical seabird colonies. Atmospheric Environment, 89: 35-42.

Riddick, S.N. et al., 2016b. Measurement of ammonia emissions from temperate and sub-polar seabird colonies. Atmospheric Environment, 134: 40-50.

Ro, K.S., Johnson, M.H., Hunt, P.G. and Flesch, T.K., 2011. Measuring Trace Gas Emission from Multi-Distributed Sources Using Vertical Radial Plume Mapping (VRPM) and Backward Lagrangian Stochastic (bLS) Techniques. Atmosphere, 2(3): 553-566.

Sanz, A., Misselbrook, T., Sanz, M.J. and Vallejo, A., 2010. Use of an inverse dispersion technique for estimating ammonia emission from surface-applied slurry. Atmospheric Environment, 44(7): 999-1002.

Sintermann, J. et al., 2011a. Determination of field scale ammonia emissions for common slurry spreading practice with two independent methods. Atmospheric Measurement Techniques, 4(9): 1821-1840.

Sintermann, J. et al., 2012. Are ammonia emissions from field-applied slurry substantially over-estimated in European emission inventories? Biogeosciences, 9(5): 1611-1632.

Sintermann, J. et al., 2011b. Eddy covariance flux measurements of ammonia by high temperature chemical ionisation mass spectrometry. Atmospheric Measurement Techniques, 4(3): 599-616.

Sommer, S.G. et al., 2003. Processes controlling ammonia emission from livestock slurry in the field. European Journal of Agronomy, 19(4): 465-486.

Sommer, S.G., Jensen, L.S., Clausen, S.B. and SØGaard, H.T., 2006. Ammonia volatilization from surface-applied livestock slurry as affected by slurry composition and slurry infiltration depth. The Journal of Agricultural Science, 144(3): 229-235.

Sommer, S.G., McGinn, S.M. and Flesch, T.K., 2005. Simple use of the backwards Lagrangian stochastic dispersion technique for measuring ammonia emission from small field-plots. European Journal of Agronomy, 23(1): 1-7.

Spirig, C., Flechard, C.R., Ammann, C. and Neftel, A., 2010. The annual ammonia budget of fertilised cut grassland - Part 1: Micrometeorological flux measurements and emissions after slurry application. Biogeosciences, 7(2): 521-536.

Sun, K. et al., 2015. Open-path eddy covariance measurements of ammonia fluxes from a beef cattle feedlot. Agricultural and Forest Meteorology, 213: 193-202.

Sutton, M.A. et al., 2001. Comparison of low cost measurement techniques for long-term monitoring of atmospheric ammonia. J Environ Monit, 3(5): 446-53.

900 Sutton, M.A. et al., 2009. Dynamics of ammonia exchange with cut grassland: synthesis of results and
901 conclusions of the GRAMINAE Integrated Experiment. Biogeosciences, 6(12): 2907-2934.
902 Sutton, M.A. et al., 2011. Too much of a good thing. Nature, 472(7342): 159-161.
903 Sutton, M.A. et al., 2013. Towards a climate-dependent paradigm of ammonia emission and deposition. Philos
904 Trans R Soc Lond B Biol Sci, 368(1621): 20130166.
905 Tang, Y.S., Cape, J.N. and Sutton, M.A., 2001. Development and types of passive samplers for monitoring
906 atmospheric NO2 and NH3 concentrations. TheScientificWorldJournal, 1: 513-29.
907 Tang, Y.S. et al., 2009. European scale application of atmospheric reactive nitrogen measurements in a low-cost
908 approach to infer dry deposition fluxes. Agriculture Ecosystems & Environment, 133(3-4): 183-195.
909 Theobald, M.R., Crittenden, P.D., Tang, Y.S. and Sutton, M.A., 2013. The application of inverse-dispersion and
910 gradient methods to estimate ammonia emissions from a penguin colony. Atmospheric Environment,
911 81: 320-329.
912 Thomson, L.C. et al., 2007. An improved algorithm for locating a gas source using inverse methods.
913 Atmospheric Environment, 41(6): 1128-1134.
914 UNECE (Editor), 2012. 1999 Protocol to Abate Acidification, Eutrophication and Ground-level Ozone to the
915 Convention on Long-range Transboundary Air Pollution, as amended on 4 May 2012
916 (http://www.unece.org/env/lrtap/multi_h1.html). UNECE, Brussels, Belgium.
917 Vandré, R. and Kaupenjohann, M., 1998. In Situ Measurement of Ammonia Emissions from Organic Fertilizers
918 in Plot Experiments. Soil Science Society of America Journal, 62(2): 467-473.
919 Wang, W., Liu, W.Q., Zhang, T.S. and Ren, M.Y., 2013. Evaluation of backward Lagrangian stochastic (bLS)
920 model to estimate gas emissions from complex sources based on numerical simulations. Atmospheric
921 Environment, 67: 211-218.
922 Whitehead, J.D. et al., 2008. Evaluation of laser absorption spectroscopic techniques for eddy covariance flux
923 measurements of ammonia. Environ Sci Technol, 42(6): 2041-6.
924 Wilson, J.D., 2015. Computing the Flux Footprint. Boundary-Layer Meteorology, 156(1): 1-14.
925 Wilson, J.D. and Shum, W.K.N., 1992. A Reexamination of the Integrated Horizontal Flux Method for
926 Estimating Volatilization from Circular Plots. Agricultural and Forest Meteorology, 57(4): 281-295.
927 Yee, E., 2008. Theory for reconstruction of an unknown number of contaminant sources using probabilistic
928 inference. Boundary-Layer Meteorology, 127(3): 359-394.
929 Yee, E. and Flesch, T.K., 2010. Inference of emission rates from multiple sources using Bayesian probability
930 theory. J Environ Monit, 12(3): 622-34.
931